Density of states functions for photonic crystals

R. C. McPhedran,[1] L. C. Botten,[2] J. McOrist,[1] A. A. Asatryan,[2] C. M. de Sterke,[1]
and N. A. Nicorovici[1]
[1]*CUDOS & School of Physics, University of Sydney, New South Wales 2006, Australia*
[2]*CUDOS & School of Mathematical Sciences, University of Technology, Sydney, New South Wales 2007, Australia*
(Received 29 May 2003; published 29 January 2004)

We discuss density of states functions for photonic crystals, in the context of the two-dimensional problem for arrays of cylinders of arbitrary cross section. We introduce the mutual density of states (MDOS), and show that this function can be used to calculate both the local density of states (LDOS), which gives position information for emission of radiation from photonic crystals, and the spectral density of states (SDOS), which gives angular information. We establish the connection between MDOS, LDOS, SDOS and the conventional density of states, which depends only on frequency. We relate all four functions to the band structure and propagating states within the crystal, and give numerical examples of the relation between band structure and density of states functions.

DOI: 10.1103/PhysRevE.69.016609 PACS number(s): 42.70.Qs, 32.80.−t, 42.50.Dv

I. INTRODUCTION

The electromagnetic properties of photonic crystals now constitute an intensive area of theoretical, numerical, and experimental effort [1]. The two earliest papers on this topic [2,3] both highlighted the ability of the photonic crystal to modify the emission or absorption properties of an atom or molecule placed within it, through differences in the density of states within the crystal from its free space value. Given the remarkable progress in the last decade in the fabrication of photonic crystals, we are now at the stage where devices such as microlasers [4] are being fabricated. Optimal design of devices relying on the emission and absorption properties of atoms within photonic crystals will require full characterization of density of state functions within them.

In its turn the density of states can be effectively deduced from the knowledge of the Green function of the corresponding problem [5]. Therefore the knowledge of the Green function is essential for the complete characterization of the radiating properties of the system. Note that the Green function and the Green's function method are one of the central elements in solid state physics [6]. The dynamic lattice Green functions are discussed in Refs. [7,8], while the static lattice Green function is considered in Ref. [9]. In contrast to the Green functions defined in these references, here we use phased or quasiperiodic Green functions, in which the source acquires an additional phase shift in moving from one unit cell to the other. This phased array of sources has been used earlier to model surface acoustic wave devices [10]. Below we show that these quasiperiodic Green functions contain comprehensive information about the emitting properties of sources embedded in periodic arrays and give rise to different density of states functions.

It is our purpose here to present a unified treatment of the classical electromagnetic calculation of density of states functions within photonic crystals. We stress at the outset that the density of states, as used in Fermi's Golden rule, arises from a semiclassical treatment of radiation by atoms, in which the atom is treated quantum mechanically, whereas the electromagnetic fields with which it interacts can be treated classically. We choose to consider the two-dimensional case, where we have line absorbers or emitters of infinite length embedded in an array of cylinders of infinite length. This has the effect of simplifying the theoretical development, for example, in permitting it to be carried out through the calculation of a single scalar field component rather than requiring a full vector treatment, but the essential features of our treatment carry over to point sources in an array of cylinders or in a lattice of spheres.

The environment of this photonic crystal influences the ability of atoms to emit and absorb radiation of a particular frequency. This influence is a function of position in the crystal, and also depends on the angular distribution of the radiation being emitted or absorbed. The dependence on the source position vector $\mathbf{r}_s$ is encapsulated in the local density of states (LDOS), which is a function of frequency ω and $\mathbf{r}_s$, while the angular distribution is encapsulated in the spectral density of states (SDOS), depending on ω and the wave vector $\mathbf{k}_0$. These two functions are much more informative than the density of states (DOS), which is a function of ω alone, but in many situations one may wish to combine both positional and angular information for radiation problems in photonic crystals. This is achieved by calculating the mutural density of states (MDOS), depending on ω, $\mathbf{r}_s$, and $\mathbf{k}_0$, which we introduce here. We show that the MDOS $\mathcal{M}(\mathbf{r}_s,\omega,\mathbf{k}_0)$ is a positive function, whose integral over the Brillouin zone (BZ) gives the LDOS, while its (weighted) integral over the Wigner-Seitz cell (WSC) gives the SDOS. If it is integrated over both cells, the result is the DOS. We study the density of states functions using Green's functions, and also using the basis of Bloch functions, which provides a convenient tool for establishing formally the links between the various functions. We show that the LDOS and SDOS are independent functions, not being a Fourier transform pair, for example, and that neither incorporates all the information present in the MDOS. We also emphasize the connections of the four density of state functions with the band structure of the photonic crystal, and discuss their dependence on polarization. The density of state functions and their relationships

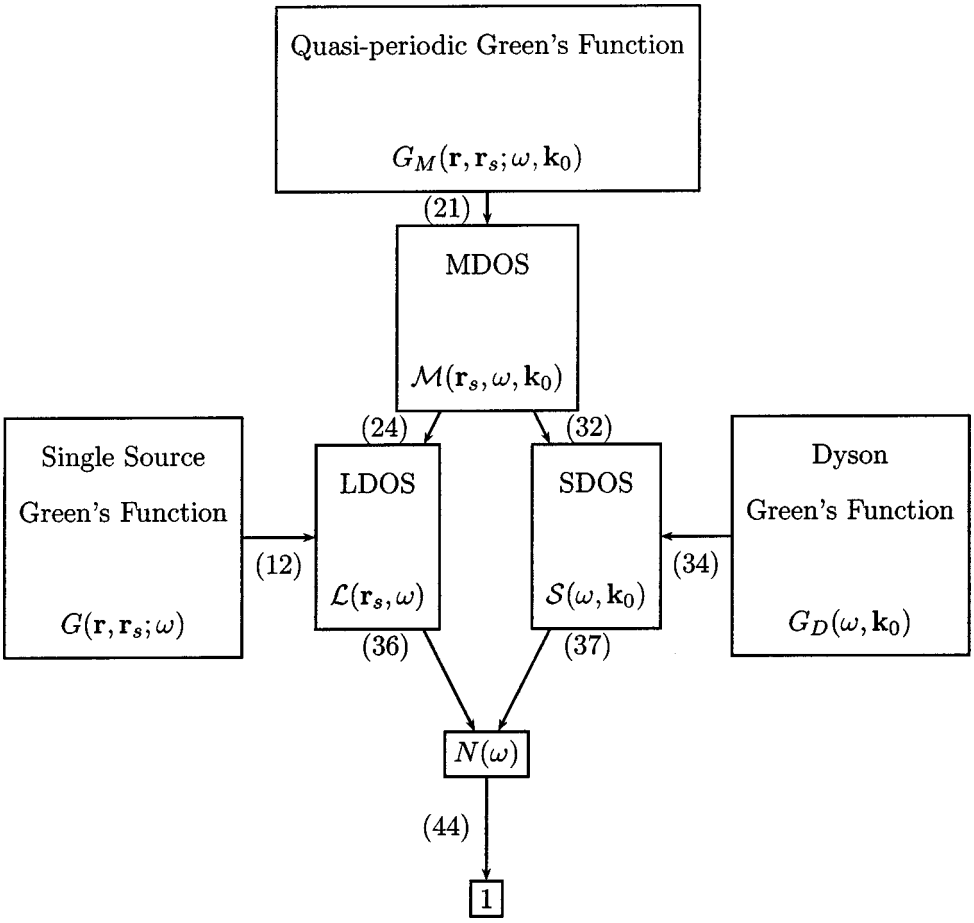

FIG. 1. Relationship between the various Green's functions and density of states functions, with relevant equation numbers.

with each other and with Green functions are shown in Fig. 1.

For a previous discussion of LDOS, SDOS, and DOS, see the review paper by Lagendijk and van Tiggelen [11]. This emphasizes the similarities and differences between quantum mechanical treatments of electrons in structured materials and the electromagnetic problem, but is oriented more towards random distributions of scatterers than the ordered case of the photonic crystal considered here. The definitions of some density of state functions have not yet become fixed by wide usage. However, the DOS is clearly defined, and subject to a normalization condition. We choose our normalizations for the LDOS and SDOS to ensure they reduce to the DOS when they are functions of frequency alone (i.e., they are independent of $\mathbf{r}_s$ and $\mathbf{k}_0$, respectively).

In the following section, we define the quasiperiodic Green's function, and express it in terms of the complete basis of Bloch functions. We then proceed to the definition of the mutual density of states, and its connections with the other density of states functions shown in Fig. 1. In the following section, we use Green's theorem to relate the group velocity, energy density, and flux of Bloch modes in photonic crystals. We next explore methods for numerical calculation of band structures and density of state functions in photonic crystals. While the bulk of this paper is concerned with TM polarization, we indicate concisely in Sec. VI how the key results should be changed for TE polarization, before making concluding remarks.

II. GREEN'S FUNCTIONS AND THE BLOCH BASIS

We consider a two-dimensional periodic function describing a real but otherwise arbitrary refractive index distribution $n(\mathbf{r})$. We define the quasiperiodic Green function that obeys the equation

$$\nabla^2 G_M(\mathbf{r},\mathbf{r}_s;\omega,\mathbf{k}_0)+\frac{\omega^2}{c^2}n^2(\mathbf{r})G_M(\mathbf{r},\mathbf{r}_s;\omega,\mathbf{k}_0)$$

$$=\sum_{p=-\infty}^{\infty}\delta(\mathbf{r}-\mathbf{r}_s-\mathbf{R}_p)e^{i\mathbf{k}_0\cdot\mathbf{R}_p}. \quad (1)$$

together with appropriate conditions for that polarization on the cylinder boundary. Here, if p denotes the integer pair n,m, $\mathbf{R}_p=n\mathbf{e}_1+m\mathbf{e}_2$, where $\mathbf{e}_1$, $\mathbf{e}_2$ are the basis vectors of the array, which has a unit cell of area A_{WSC} and a Brillouin zone of area A_{BZ}. Also, the function $n(\mathbf{r})$ is periodic in position, as is its square, $\varepsilon(\mathbf{r})$. Note that the vector $\mathbf{k}_0$ defines the quasiperiodicity or Bloch property of the Green's function, either in terms of the field vector $\mathbf{r}$,

$$G_M(\mathbf{r}+\mathbf{R}_p,\mathbf{r}_s,\omega,\mathbf{k}_0)=G_M(\mathbf{r},\mathbf{r}_s;\omega,\mathbf{k}_0)e^{i\mathbf{k}_0\cdot\mathbf{R}_p}, \quad (2)$$

or in terms of the vector $\mathbf{r}_s$ specifying the position of the source in the central unit cell:

$$G_M(\mathbf{r},\mathbf{r}_s+\mathbf{R}_p,\omega,\mathbf{k}_0)=G_M(\mathbf{r},\mathbf{r}_s;\omega,\mathbf{k}_0)e^{-i\mathbf{k}_0\cdot\mathbf{R}_p}. \quad (3)$$

We recall at this point two forms of the Poisson summation formula [12]

$$A_{WSC}\sum_p \delta(\mathbf{r}-\mathbf{r}_s-\mathbf{R}_p)e^{i\mathbf{k}_0\cdot\mathbf{R}_p}=\sum_h e^{i\mathbf{Q}_h\cdot(\mathbf{r}-\mathbf{r}_s)}, \quad (4)$$

giving the plane wave representation of a sum of point sources, and its reciprocal form

$$A_{\mathrm{BZ}}\sum_h \delta(\mathbf{k}-\mathbf{Q}_h)=\sum_p e^{i\mathbf{R}_p\cdot(\mathbf{k}-\mathbf{k}_0)}. \quad (5)$$

In Eq. (4), $\mathbf{Q}_h=\mathbf{K}_h+\mathbf{k}_0$ runs over plane waves with the correct quasiperiodicity ($\mathbf{K}_h$ specifying the set of all reciprocal lattice vectors). Thus, we can rewrite (1) with its source term as a sum of plane waves:

$$\nabla^2 G_M(\mathbf{r},\mathbf{r}_s;\omega,\mathbf{k}_0)+\frac{\omega^2}{c^2}n^2(\mathbf{r})G_M(\mathbf{r},\mathbf{r}_s;\omega,\mathbf{k}_0)$$

$$=\frac{1}{A_{WSC}}\sum_h e^{i\mathbf{Q}_h\cdot(\mathbf{r}-\mathbf{r}_s)}. \quad (6)$$

To be definite, we will consider $E_\parallel$ or TM polarization, so that G_M refers to the z component of the electric field, with G_M and its normal derivative $\partial G_M/\partial n$ being continuous at interfaces. For $H_\parallel$ polarization, G_M and $(1/\varepsilon)\partial G_M/\partial n$ are continuous.

Equations (1) and (6) define an inhomogeneous or source problem. We can also consider the homogeneous problem, whose solutions are the Bloch functions or photonic modes for the array:

$$\nabla^2\psi_m(\mathbf{k}_0,\mathbf{r})+\frac{\omega_m^2}{c^2}n^2(\mathbf{r})\psi_m(\mathbf{k}_0,\mathbf{r})=0, \quad (7)$$

together with the boundary conditions on the cylinder (ψ_m, $\partial\psi_m/\partial n$ continuous) and the quasiperiodicity condition

$$\psi_m(\mathbf{k}_0,\mathbf{r}+\mathbf{R}_p)=\psi_m(\mathbf{k}_0,\mathbf{r})e^{i\mathbf{k}_0\cdot\mathbf{R}_p}. \quad (8)$$

Note that the frequency for the mth mode is determined by the differential equation (7), the quasiperiodicity condition (8) and the boundary conditions, so that $\omega_m=\omega_m(\mathbf{k}_0)$.

The functions $\psi_m(\mathbf{k}_0,\mathbf{r})$ are orthogonal with respect to the inner product

$$\langle\psi_l,\psi_m\rangle=\int_{\mathrm{WSC}}\varepsilon(\mathbf{r})\psi_l(\mathbf{k}_0,\mathbf{r})\psi_m^*(\mathbf{k}_0,\mathbf{r})d^2\mathbf{r}, \quad (9)$$

as is readily proved using Green's theorem. We will assume that the set of Bloch functions for a fixed $\mathbf{k}_0$ form a complete, normalized basis of functions. Some relevant properties and references to previous relevant work may be found in the paper by Allaire, Conca, and Vanninathan [13]. For example, we can expand any quasiperiodic solution $f(\mathbf{k}_0,\mathbf{r})$ of the Helmholtz equation in terms of ψ_m as

$$f(\mathbf{k}_0,\mathbf{r})=\sum_l c_l\psi_l(\mathbf{k}_0,\mathbf{r}), \quad (10)$$

where from Eq. (9),

$$c_l=\int_{\mathrm{WSC}}\varepsilon(\mathbf{r})f(\mathbf{k}_0,\mathbf{r})\psi_l^*(\mathbf{k}_0,\mathbf{r})d^2\mathbf{r}. \quad (11)$$

Applying Eqs. (10) and (11) to the right-hand side of Eq. (1), we obtain

$$\sum_{p=-\infty}^{\infty}\delta(\mathbf{r}-\mathbf{r}_s-\mathbf{R}_p)e^{i\mathbf{k}_0\cdot\mathbf{R}_p}=\sum_l n^2(\mathbf{r}_s)\psi_l^*(\mathbf{k}_0,\mathbf{r}_s)\psi_l(\mathbf{k}_0,\mathbf{r}). \quad (12)$$

The asymmetry in Eq. (12) between $\mathbf{r}$ and $\mathbf{r}_s$ is misleading, since the left- and right-hand sides are only nonzero if $\mathbf{r}=\mathbf{r}_s+\mathbf{R}_p$, which guarantees that $n^2(\mathbf{r})=n^2(\mathbf{r}_s)$. Using the expansion (12) on the right-hand side of Eq. (1), we can obtain the expansion of the Green's function G_M in terms of the Bloch functions $\psi_l(\mathbf{k}_0,\mathbf{r})$ as

$$G_M(\mathbf{r},\mathbf{r}_s;\omega,\mathbf{k}_0)=\sum_l \frac{n^2(\mathbf{r}_s)\psi_l^*(\mathbf{k}_0,\mathbf{r}_s)\psi_l(\mathbf{k}_0,\mathbf{r})}{n^2(\mathbf{r})[\omega^2-\omega_l^2(\mathbf{k}_0)]/c^2}. \quad (13)$$

Using the Plemelj formula

$$\frac{1}{x-x_0+i\eta}=\mathrm{P}\frac{1}{x-x_0}-i\pi\delta(x-x_0), \quad (14)$$

we arrive at

$$G_M(\mathbf{r},\mathbf{r}_s;\omega,\mathbf{k}_0)$$

$$=\mathrm{P}G_M-\frac{i\pi c^2 n^2(\mathbf{r}_s)}{2\omega n^2(\mathbf{r})}\sum_m \psi_m^*(\mathbf{k}_0,\mathbf{r}_s)\psi_m(\mathbf{k}_0,\mathbf{r})$$

$$\times\delta(\omega-\omega_m(\mathbf{k}_0,\mathbf{r})). \quad (15)$$

Here, P denotes the Cauchy principal value. Note that, when $\mathbf{r}=\mathbf{r}_s$, the second term on the right-hand side of Eq. (15) is purely imaginary since the product $\psi\psi^*$ then becomes $|\psi|^2$. So the two terms on the right-hand side of Eq. (15) then correspond to real and imaginary parts, respectively.

III. DENSITY OF STATES FUNCTIONS

One way to calculate density of states functions (see the left side of Fig. 1) is through the imaginary part of the Green's function, evaluated when the field point coincides with the source point (under those circumstances, of course, the real part becomes singular). For example, we can construct the LDOS $\mathcal{L}(\mathbf{r}_s;\omega)$ from a Green's function $G(\mathbf{r},\mathbf{r}_s;\omega)$ which corresponds to a single source, rather than the quasiperiodic superposition of sources evident in Eq. (1):

$$\nabla^2 G(\mathbf{r},\mathbf{r}_s;\omega)+\frac{\omega^2}{c^2}n^2(\mathbf{r})G(\mathbf{r},\mathbf{r}_s;\omega)=\delta(\mathbf{r}-\mathbf{r}_s). \quad (16)$$

Given G, $\mathcal{L}$ follows from the definition [8]

$$\mathcal{L}(\mathbf{r}_s;\omega)=-\frac{2\omega}{\pi c^2}\mathrm{Im}\ [\mathbf{G}(\mathbf{r}_s,\mathbf{r}_s;\omega)]\ \mathcal{U}, \quad (17)$$

where $\mathcal{U}$ is the normalization factor,

$$\mathcal{U}=\int_{\mathrm{WSC}}\varepsilon(\mathbf{r}_s)d^2\mathbf{r}_s, \quad (18)$$

corresponding to the dielectric constant integrated over the Wigner-Seitz cell.

We will now establish the relationship between G_M and G shown in Fig. 1. The integral of the Bloch factor occurring on the right-hand side of Eq. (1) over the Brillouin zone is zero unless the lattice vector $\mathbf{R}_p$ is zero:

$$\frac{1}{A_{\mathrm{BZ}}}\int_{\mathrm{BZ}}\exp(i\mathbf{k_0}\cdot\mathbf{R}_p)d^2\mathbf{k_0}=\delta_{p,0}, \quad (19)$$

where A_{BZ} is the area of the Brillouin zone. Hence, G is obtained from G_M by integration

$$G(\mathbf{r},\mathbf{r}_s;\omega)=\frac{1}{A_{\mathrm{BZ}}}\int_{\mathrm{BZ}}G_M(\mathbf{r},\mathbf{r}_s;\omega,\mathbf{k}_0)d^2\mathbf{k}_0. \quad (20)$$

We can now define the mutual density of states by analogy with the local density of states (17):

$$\mathcal{M}(\mathbf{r}_s,\omega,\mathbf{k}_0)=-\frac{2\omega}{\pi c^2}\mathrm{Im}\ [G_M(\mathbf{r}_s,\mathbf{r}_s,\omega,\mathbf{k}_0)]\ \mathcal{U}$$
$$=\sum_m\ \delta(\omega-\omega_m(\mathbf{k}_0))|\psi_m(\mathbf{k}_0,\mathbf{r}_s)|^2\ \mathcal{U}, \quad (21)$$

where the summation goes over all modes m of the photonic crystal and $\psi_m(\mathbf{k}_0,\mathbf{r}_s)$ is the eigenfunction normalized according to

$$\int_{\mathrm{WSC}}\varepsilon(\mathbf{r}_s)|\psi_m(\mathbf{k}_0,\mathbf{r}_s)|^2d^2\mathbf{r}_s=1. \quad (22)$$

Thus, the MDOS is a non-negative function, which is zero in any band gap, i.e., in any range of ω in which there are no propagating modes of frequency $\omega_m(\mathbf{k}_0)$.

In keeping with Eq. (20), we integrate Eq. (21) over the Brillouin zone:

$$\frac{1}{A_{\mathrm{BZ}}}\int_{\mathrm{BZ}}\mathcal{M}(\mathbf{r}_s,\omega,\mathbf{k}_0)d^2\mathbf{k}_0$$
$$=-\frac{2\omega\mathcal{U}}{A_{\mathrm{BZ}}\pi c^2}\int_{\mathrm{BZ}}d^2\mathbf{k}_0\mathrm{Im}G_M(\mathbf{r}_s,\mathbf{r}_s,\omega,\mathbf{k}_0) \quad (23)$$

or, using Eq. (17),

$$\frac{1}{A_{\mathrm{BZ}}}\int_{\mathrm{BZ}}\mathcal{M}(\mathbf{r}_s,\omega,\mathbf{k}_0)d^2\mathbf{k}_0$$
$$=-\frac{2\omega\mathcal{U}}{\pi c^2}\mathrm{Im}G(\mathbf{r}_s,\mathbf{r}_s,\omega)=\mathcal{L}(\mathbf{r}_s,\omega). \quad (24)$$

Thus, the LDOS follows from the MDOS by integration over the Brillouin zone:

$$\mathcal{L}(\mathbf{r}_s,\omega)=\frac{\mathcal{U}}{A_{\mathrm{BZ}}}\sum_m\ \int_{\mathrm{BZ}}d^2\mathbf{k}_0\delta(\omega-\omega_m(\mathbf{k}_0))|\psi_m(\mathbf{k}_0,\mathbf{r}_s)|^2. \quad (25)$$

From Eq. (25), we see that the LDOS obeys the same boundary conditions as the functions ψ, i.e., both this and its normal derivative are continuous across cylinder boundaries. It is a non-negative function throughout the Wigner-Seitz cell, and is periodic. However, it does not obey the Helmholtz equation. In fact, it satisfies

$$\left[\nabla^2+2\frac{\omega^2}{c^2}n^2(\mathbf{r})\right]\mathcal{L}(\mathbf{r}_s,\omega)$$
$$=\frac{2\mathcal{U}}{A_{\mathrm{BZ}}}\sum_m\ \int_{\mathrm{BZ}}\delta(\omega-\omega_m)\boldsymbol{\nabla}\psi_m(\mathbf{k}_0,\mathbf{r}_s)$$
$$\cdot\boldsymbol{\nabla}\psi_m^*(\mathbf{k}_0,\mathbf{r}_s)d^2\mathbf{k}_0, \quad (26)$$

where $\omega_m=\omega_m(\mathbf{k}_0)$. The interpretation of Eq. (26) is that the source of the LDOS is the combined electromagnetic energy density of all propagating modes.

Another physical interpretation of the LDOS can be deduced from Green's theorem applied to the unit cell containing the primary source

$$\int\int(G\nabla^2G^*-G^*\nabla^2G)dA$$
$$=\left(\int_\Gamma-\int_C\right)\left(G\frac{\partial G^*}{\partial n}-G\frac{\partial G^*}{\partial n}\right)ds. \quad (27)$$

Taking the source to be in the exterior region U_+ of Fig. 2, the left-hand side of Eq. (27) reduces to $2i\mathrm{Im}[G_M(\mathbf{r}_s,\mathbf{r}_s)]$. The contour integral around C on the right-hand side of Eq. (27) can be shown to vanish for lossless media after applying the continuity conditions on C and again applying Green's theorem to the interior region U_-. Thus

$$2i\ \ \mathrm{Im}[G(\mathbf{r}_s,\mathbf{r}_s,\omega)]=\int_\Gamma\left(G\frac{\partial G^*}{\partial n}-G\frac{\partial G^*}{\partial n}\right)ds. \quad (28)$$

The integral on the right-hand side of Eq. (28) is proportional to the outgoing flux through Γ due to the source and we deduce

$$2i\mathrm{Im}[G(\mathbf{r}_s,\mathbf{r}_s,\omega)]=-2kZ_0\mathcal{F}, \quad (29)$$

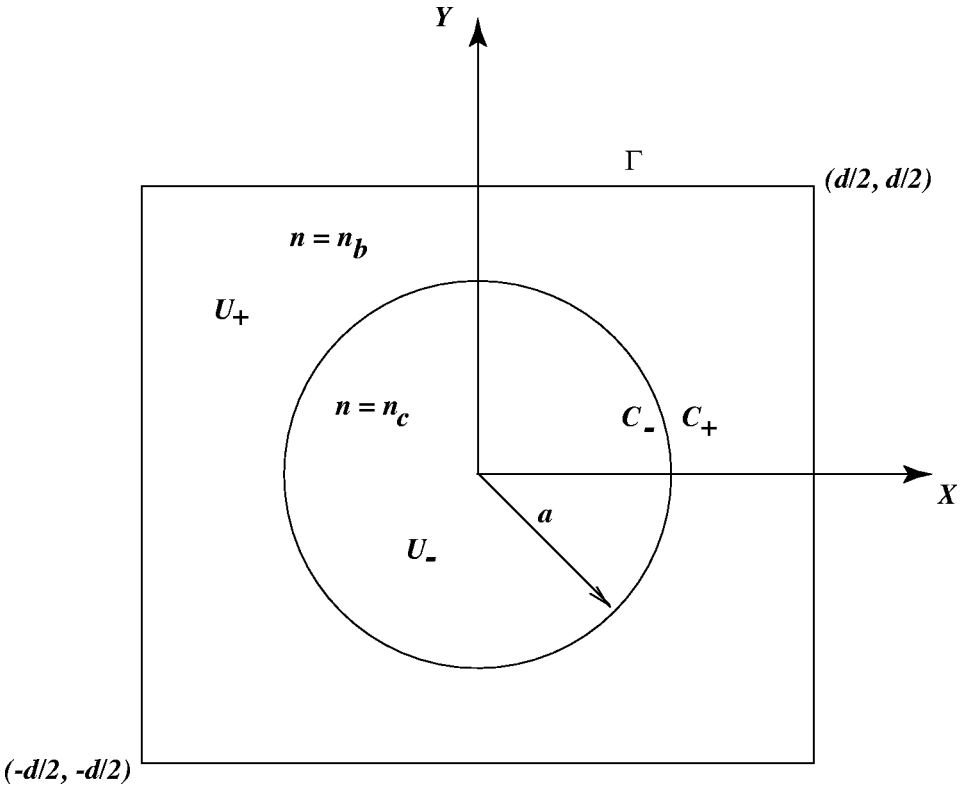

FIG. 2. The geometry for the application of Green's theorem. A cylinder of radius $r=a$ has a contour C_- just inside its surface and C_+ just outside. The unit cell has bounding contour Γ, and area U, divided by C into U_- and U_+.

where $\mathcal{F}$ is the outgoing flux and Z_0 is the impedance of free space. Thus, the energy that can be extracted from the source depends directly on the available density of modes given by the MDOS:

$$\mathcal{L}(\mathbf{r}_s,\omega)=-\frac{2\omega}{\pi c^2}\mathrm{Im}[G_M(\mathbf{r}_s,\mathbf{r}_s,\omega)]=\frac{4k^2\mu_0}{\pi}\mathcal{F}. \quad (30)$$

We now move to the right-hand side of Fig. 1, and integrate (21) over the WSC:

$$\frac{1}{\mathcal{U}}\int_{\mathrm{WSC}}\varepsilon(\mathbf{r}_s)\mathcal{M}(\mathbf{r}_s,\omega,\mathbf{k}_0)d^2\mathbf{r}_s = \sum_m \delta(\omega-\omega_m(\mathbf{k}_0))\int_{\mathrm{WSC}}\varepsilon(\mathbf{r}_s)|\psi_m(\mathbf{k}_0,\mathbf{r}_s)|^2 d^2\mathbf{r}_s. \quad (31)$$

Hence,

$$\frac{1}{\mathcal{U}}\int_{\mathrm{WSC}}d^2\mathbf{r}_s\varepsilon(\mathbf{r}_s)\mathcal{M}(\mathbf{r}_s,\omega,\mathbf{k}_0)=\sum_m \delta(\omega-\omega_m(\mathbf{k}_0)) = \mathcal{S}(\omega,\mathbf{k}_0). \quad (32)$$

This result is the spectral DOS $\mathcal{S}(\omega,\mathbf{k}_0)$, which is a function of frequency and position in the Brillouin zone incorporating the information contained in the complete photonic band diagram for the structure in question.

We now relate the SDOS to the Dyson Green function [11,7] $G_D(\omega,\mathbf{k}_0)$. From Eq. (13),

$$G_M(\mathbf{r}_s,\mathbf{r}_s;\omega,\mathbf{k}_0)=\sum_l \frac{c^2|\psi_l(\mathbf{k}_0,\mathbf{r}_s)|^2}{[\omega^2-\omega_l^2(\mathbf{k}_0)]}. \quad (33)$$

Hence, using the normalization condition (22)

$$\frac{1}{\mathcal{U}}\int_{\mathrm{WSC}}G_M(\mathbf{r}_s,\mathbf{r}_s;\omega,\mathbf{k}_0)\varepsilon(\mathbf{r}_s)d^2\mathbf{r}_s = \frac{c^2}{\mathcal{U}}\sum_m \frac{1}{[\omega^2-\omega_m^2(\mathbf{k}_0)]}=G_D(\omega,\mathbf{k}_0). \quad (34)$$

From the Plemelj formula (14), we arrive at the equation for the SDOS analogous to the definition (17) of the LDOS:

$$\mathcal{S}(\omega,\mathbf{k}_0)=\frac{-2\omega\mathcal{U}}{\pi c^2}\mathrm{Im}G_D(\omega,\mathbf{k}_0). \quad (35)$$

Comparing (32) and (25), we see that the SDOS is determined entirely by the dispersion equation for the bands, i.e., by their shape, with any position information having been integrated out. The LDOS is determined from the squared magnitudes of the modes, integrated over the isofrequency contours $C(\omega_m)$, representing the curves following the vectors $\mathbf{k}_0$ for which mode m has the specified frequency—i.e., $\omega=\omega_m(\mathbf{k}_0)$. Thus, the LDOS combines information concerning both the band shape and the form of the modes, but it has lost information about directional dependence through the integration over the Brillouin zone.

The total density of states is defined as

$$N(\omega)=\frac{1}{\mathcal{U}}\int_{\mathrm{WSC}}\varepsilon(\mathbf{r}_s)\mathcal{L}(r_s,\omega)d^2\mathbf{r}_s. \tag{36}$$

After substitution of Eqs. (21) and (24) into Eq. (36) and use of the normalization condition (22), we obtain

$$N(\omega)=\sum_m \frac{1}{A_{\mathrm{BZ}}}\int_{\mathrm{BZ}}\delta(\omega-\omega_m(\mathbf{k}_0))d^2\mathbf{k_0}$$

$$=\frac{1}{A_{\mathrm{BZ}}}\int_{\mathrm{BZ}}\mathcal{S}(\omega,\mathbf{k}_0)d^2\mathbf{k}_0. \tag{37}$$

Thus, we have established the two paths to the density of states $N(\omega)$ shown in Fig. 1.

Now we expand in a Taylor series in the vicinity of the isofrequency contour [i.e., the unconstrained vector $\mathbf{k}_0$ is close to the vector $\mathbf{k}_0(\omega_m)$ lying on the isofrequency contour] to give

$$\omega-\omega_m(\mathbf{k}_0)=\boldsymbol{\nabla}_{\mathbf{k}_0}\omega\cdot[\mathbf{k}_0-\mathbf{k}_0(\omega_m)]+O(|\mathbf{k}_0-\mathbf{k}_0(\omega_m)|^2). \tag{38}$$

After substitution of this equation into Eq. (37) and use of the property $\delta(ax)=\delta(x)/|a|$ we find

$$N(\omega)=\sum_m \frac{1}{A_{\mathrm{BZ}}}\int_{\mathrm{BZ}}\frac{1}{v_g}\delta(\hat{\mathbf{u}}\cdot[\mathbf{k}_0-\mathbf{k}_0(\omega_m)])d^2\mathbf{k}_0, \tag{39}$$

where $v_g=|\boldsymbol{\nabla}_{\mathbf{k}_0}\omega|$ is the group velocity and $\hat{\mathbf{u}}$ represents the unit vector in the direction of $\boldsymbol{\nabla}_{\mathbf{k}_0}\omega$ (that is, the direction normal to the isofrequency lines). To carry out the integration over the Brillouin zone, we express $\mathbf{k}_0$ as $\mathbf{k}_0=(k_{0\mathrm{t}},k_{0\mathrm{n}})$, where $k_{0\mathrm{t}}$ is the projection of $\mathbf{k}_0$ onto the tangent to an isofrequency line, while $k_{0\mathrm{n}}=\mathbf{k}_0\cdot\hat{\mathbf{u}}$. In terms of these new variables Eq. (39) takes the form

$$N(\omega)=\sum_m \frac{1}{A_{\mathrm{BZ}}}\int_{\mathrm{BZ}}\frac{1}{v_g}\delta(k_{\mathrm{n}}-k_{0,\mathrm{n}}(\omega_m))dk_{0\mathrm{t}}dk_{0\mathrm{n}}. \tag{40}$$

The integration with respect to k_{n} (in the direction normal to the isofrequency lines) can be done in closed form using the δ function and we obtain

$$N(\omega)=\sum_m \frac{1}{A_{\mathrm{BZ}}}\int_{C(\omega_m)}\frac{1}{v_g}dk_{0\mathrm{t}}, \tag{41}$$

where $C(\omega_m)$ is the isofrequency line $\omega=\omega_m$. This expression for the density of states agrees with that found in standard texts [14].

Equation (25) can be treated in a similar fashion, to give

$$\mathcal{L}(\mathbf{r}_s,\omega)=\mathcal{U}\sum_m \frac{1}{A_{\mathrm{BZ}}}\int_{C(\omega_m)}\frac{|\psi_m(\mathbf{k}_0,\mathbf{r}_s)|^2}{v_g}dk_{0\mathrm{t}}. \tag{42}$$

Of course, if we substitute Eq. (42) into Eq. (36) and use the normalization condition (22), we return to the expression (41).

We can also integrate Eq. (26) over the Wigner-Seitz cell. The term involving the Laplacian integrates to zero because of the periodicity of $\mathcal{L}(\mathbf{r}_s,\omega)$, and the other two terms are both proportional to the density of states $N(\omega)$. The result is an alternate way of expressing the normalization condition (22):

$$\int_{\mathrm{WSC}}\boldsymbol{\nabla}\psi_m(\mathbf{k}_0,\mathbf{r}_s)\cdot\boldsymbol{\nabla}\psi_m^*(\mathbf{k}_0,\mathbf{r}_s)d^2\mathbf{r}_s=\frac{\omega_m^2}{c^2}. \tag{43}$$

We define the photonic band m as the surface for mode m defined by the single-valued function $\omega_m(\mathbf{k}_0)$ as $\mathbf{k}_0$ runs over the Brillouin zone. We note that the single-valued nature of the mode dispersion relation is guaranteed since the photonic band cannot have folds, and this in turn follows from the necessity for the group velocity to remain finite. Of course, as the frequency increases, so does the tendency to have band surfaces which pass through each other. However, the absence of folds means we can always disentangle intersecting bands. Then, from Eq. (37),

$$\int_{\text{band m}}N(\omega)d\omega=\frac{1}{A_{\mathrm{BZ}}}\int_{\mathrm{BZ}}d^2\mathbf{k_0}\int_{\text{band m}}\delta(\omega-\omega_m(\mathbf{k}_0))d\omega$$

$$=\frac{1}{A_{\mathrm{BZ}}}\int_{\mathrm{BZ}}d^2\mathbf{k}_0=1. \tag{44}$$

Each band thus contributes one state to the integrated DOS, completing Fig. 1.

In the Appendix, we illustrate these results by calculating the various density of states functions for the case of periodic boundary conditions, but with a uniform refractive index (i.e., $n_c=n_b$). There the effect of the normalization factor $\mathcal{U}$ can be seen, in that the LDOS and DOS coincide.

We note that, from Eq. (21), the function $\mathcal{M}$ is periodic in both $\mathbf{k}_0$ and $\mathbf{r}$, as well as being real valued and non-negative. It follows that it, and equally well $\varepsilon\mathcal{M}$, can be expanded in series involving both the reciprocal $\mathbf{K}_h$ and direct bases $\mathbf{R}_p$:

$$\varepsilon(\mathbf{r}_s)\mathcal{M}(\mathbf{r}_s,\omega,\mathbf{k}_0)=\sum_{p,h}m_{p,h}e^{i(\mathbf{K}_h\cdot\mathbf{r}_s+\mathbf{k}_0\cdot\mathbf{R}_p)}, \tag{45}$$

where $m_{p,h}$ are appropriate expansion coefficients. Hence, we see that

$$\varepsilon(\mathbf{r}_s)\mathcal{L}(\mathbf{r}_s,\omega)=\frac{1}{A_{\mathrm{BZ}}}\int_{\mathrm{BZ}}\sum_{p,h}m_{p,h}e^{i(\mathbf{K}_h\cdot\mathbf{r}_s)}e^{i(\mathbf{k}_0\cdot\mathbf{R}_p)}d^2\mathbf{k}_0, \tag{46}$$

and, using Eq. (19), we find the following Fourier series in reciprocal space:

$$\varepsilon(\mathbf{r}_s)\mathcal{L}(\mathbf{r}_s,\omega)=\sum_h m_{0,h}e^{i(\mathbf{K}_h\cdot\mathbf{r}_s)}. \tag{47}$$

For the spectral density of states, we use Eq. (32),

$$\mathcal{S}(\omega,\mathbf{k}_0)=\frac{1}{\mathcal{U}}\int_{\mathrm{WSC}}\varepsilon(\mathbf{r}_s)\mathcal{M}(\mathbf{r}_s,\omega,\mathbf{k}_0)d^2\mathbf{r}_s. \tag{48}$$

Using Eq. (45) in Eq. (48), we find the following Fourier series in direct space:

$$\mathcal{S}(\omega,\mathbf{k}_0)=\frac{A_{\mathrm{WSC}}}{\mathcal{U}}\sum_p m_{p,0}e^{i\mathbf{k}_0\cdot\mathbf{R}_p}. \tag{49}$$

Hence,

$$N(\omega)=\frac{A_{\mathrm{WSC}}}{\mathcal{U}}m_{0,0}. \tag{50}$$

Note that the Fourier series for the local DOS (47) and the spectral DOS (49) involve disjunct sets of the Fourier coefficients of $\mathcal{M}$, with the only element in common (the $m_{0,0}$ term) determining the density of states.

IV. ENERGY, FLUX, AND GROUP VELOCITY

We now specialize to the case where the inclusions are circular cylinders of refractive index n_c in a matrix or background material of index n_b, as in Fig. 2. Given a mode ψ_m found from the homogeneous problem (7) and (8), we need to normalize it to give

$$\mathcal{N}_m=\langle\psi_m,\psi_m\rangle=\int_{\mathrm{WSC}}\varepsilon(\mathbf{r})\psi_m(\mathbf{k}_0,\mathbf{r})\psi_m^*(\mathbf{k}_0,\mathbf{r})d^2\mathbf{r}=1. \tag{51}$$

Rather than achieve this through numerical evaluation of a double integral, we can use Green's theorem to obtain the normalization in terms of a sum over expansion coefficients of the homogeneous solution. The analysis also will lead us to a useful relationship linking the energy flux carried by a mode through a boundary of the unit cell to its energy and group velocity.

We apply Green's theorem to a pair of modes ψ_m, ψ_m', corresponding to the same quasiperiodicity vector $\mathbf{k}_0$, but to cylinders of refractive index n_c, n_c', respectively. The difference in index $n_c'-n_c=\delta n$ is associated with a difference in frequency $\delta\omega=\omega_m'-\omega_m$. Then

$$\begin{aligned}\int_U(\psi_m'^*\nabla^2\psi_m-\psi_m\nabla^2\psi_m'^*)dA&=\int_\Gamma\left(\psi_m'^*\frac{\partial\psi_m}{\partial n}-\psi_m\frac{\partial\psi_m'^*}{\partial n}\right)dl\\&+\int_{C_-}\left[\psi_m'^*\frac{\partial\psi_m}{\partial n}-\psi_m\frac{\partial\psi_m'^*}{\partial n}\right]_{r=a}ad\theta\\&-\int_{C_+}\left[\psi_m'^*\frac{\partial\psi_m}{\partial n}-\psi_m\frac{\partial\psi_m'^*}{\partial n}\right]_{r=a}ad\theta.\end{aligned} \tag{52}$$

The integrals over C_+ and C_- cancel through the boundary conditions, while the integral over Γ gives zero because of the quasiperiodicity conditions common to ψ_m and ψ_m'. Hence,

$$\frac{(\omega_m'^2-\omega_m^2)}{c^2}\int_{U_+}\psi_m\psi_m'^*dA+\frac{(n_c'^2\omega_m'^2-n_c^2\omega_m^2)}{c^2}\int_{U_-}\psi_m\psi_m'^*dA=0. \tag{53}$$

We write

$$\omega_m'=\omega_m+\frac{\partial\omega_m}{\partial n_c}\delta n+\cdots, \tag{54}$$

and expand both terms in Eq. (53) to first order in δn. After some algebra, we find

$$\begin{aligned}\mathcal{N}&=\int_{U_+}|\psi_m|^2dA+n_c^2\int_{U_-}|\psi_m|^2dA\\&=\frac{-n_c\omega_m}{\partial\omega_m/\partial n_c}\int_{U_-}|\psi_m|^2dA.\end{aligned} \tag{55}$$

From Eq. (55), we see that $\partial\omega_m/\partial n_c<0$: increasing the cylinder index lowers the frequency of the photonic crystal bands, for $E_\parallel$ polarization, as would be expected on physical grounds.

Consider now

$$\mathcal{N}_-=n_c^2\int_{U_-}|\psi_m|^2dA. \tag{56}$$

We evaluate this using Green's theorem once more. If we consider the particular case where the cylinders have circular cross sections, we can use the expansions

$$\psi_m=\sum_l C_l^m J_l(n_c kr)e^{il\theta} \tag{57}$$

and

$$\psi_m'=\sum_l C_l^{m\prime}J_l(n_c'kr)e^{il\theta}, \tag{58}$$

to give using a first-order analysis

$$\mathcal{N}_-=\frac{-2\pi akn_cc^2}{2\omega_m(\omega_m+n_c\partial\omega_m/\partial n_c)}\sum_l|C_m^l|^2J_l(n_cka)J_l'(n_cka). \tag{59}$$

Combining Eq. (55) and (59), we find

$$\mathcal{N}=\frac{\pi akc^2}{(\partial\omega_m/\partial n_c)(\omega_m+n_c\partial\omega_m/\partial n_c)}\times\sum_l|C_m^l|^2J_l(n_cka)J_l'(n_cka). \tag{60}$$

Consider next the case where ω_m and ω_m' differ because of a difference in the x component k_{0x} of $\mathbf{k}_0$. Then from Green's theorem

$$\frac{\omega_m'^2-\omega_m^2}{c^2}\int_U n^2(\mathbf{r})\psi_m\psi_m'^* dA=\int_\Gamma\left(\psi_m'^*\frac{\partial\psi_m}{\partial n}-\psi_m\frac{\partial\psi_m'^*}{\partial n}\right)dl. \tag{61}$$

Expanding the left-hand side to leading order, we find

$$\frac{2\omega_m}{c^2}\frac{\partial\omega_m}{\partial k_{0x}}\delta k_{0x}\mathcal{N}=\int_\Gamma\left(\psi_m'^*\frac{\partial\psi_m}{\partial n}-\psi_m\frac{\partial\psi_m'^*}{\partial n}\right)dl+\cdots. \tag{62}$$

For the right-hand side, the integrals over $y=-d/2$ and $y=d/2$ cancel by the common quasiperiodicity of ψ_m and ψ_m'. Using the Bloch factors corresponding to k_{0x} and k_{0x}', we obtain for the other two sides

$$\begin{aligned}[e^{i(k_{0x}-k_{0x}')d}-1]&\int_{y=-d/2}^{d/2}\left(\psi_m'^*\frac{\partial\psi_m}{\partial n}-\psi_m\frac{\partial\psi_m'^*}{\partial n}\right)_{x=-d/2}dy\\&=-i\delta k_{0x}d\int_{y=-d/2}^{d/2}\left(\psi_m'^*\frac{\partial\psi_m}{\partial n}-\psi_m\frac{\partial\psi_m'^*}{\partial n}\right)_{x=-d/2}dy\\&\quad+\cdots.\end{aligned} \tag{63}$$

Hence, equating coefficients of δk_{0x},

$$\omega_m\frac{\partial\omega_m}{\partial k_{0x}}\mathcal{N}=c^2d\,\mathrm{Im}\left[\int_{y=-d/2}^{d/2}\left[\psi_m^*\frac{\partial\psi_m}{\partial x}\right]_{x=-d/2}dy\right]. \tag{64}$$

We interpret Eq. (64) in terms of electromagnetic energy fluxes if we evaluate the electric and magnetic fields associated with ψ_m, respectively,

$$\mathbf{E}=(0,0,\psi_m) \tag{65}$$

and

$$\mathbf{H}=\frac{ic^2}{\omega_m}\left(-\frac{\partial\psi_m}{\partial y},\frac{\partial\psi_m}{\partial x},0\right). \tag{66}$$

Hence, the Poynting vector associated with this mode is

$$\mathcal{S}=\frac{c^2}{\omega_m}\mathrm{Im}(\psi_m^*\boldsymbol{\nabla}\psi_m). \tag{67}$$

Accordingly, the flux of energy through the side of the unit cell at $x=-d/2$ is

$$\mathcal{F}_x=\frac{c^2}{\omega_m}\mathrm{Im}\left[\int_{-d/2}^{d/2}\left[\psi_m^*\frac{\partial\psi_m}{\partial x}\right]_{x=-d/2}dy\right]. \tag{68}$$

The result is that Eq. (64) becomes

$$\frac{\partial\omega_m}{\partial k_{0x}}\mathcal{N}=d\mathcal{F}_x, \tag{69}$$

or, in vector form, adding in the corresponding result for a perturbation of k_{0y},

$$\mathbf{v}_g\frac{\mathcal{N}}{d^2}=\frac{\mathcal{F}}{d}. \tag{70}$$

This result on the left-hand side is the product of the group velocity and the energy density of the mode. On the right-hand side we have the vectorial flux density associated with the mode. If we normalize the mode so that $\mathcal{N}=1$, then Eq. (70) takes the simple form that $\mathbf{v}_g=d\mathcal{F}$.

V. METHODS FOR CALCULATING DENSITY OF STATE FUNCTIONS

A. MDOS, mode, and group velocity surfaces

We start with the MDOS, which follows from Eq. (21) once the Green's function G_M is known. The calculation of G_M has been discussed by Poulton *et al.* [15], and we summarize the method here for TM polarization. It relies on multipole expansions for G_M inside the central cylinder (labeled with a superscript 0),

$$G_{M,int}(r,\theta)=\sum_{m=-\infty}^{\infty}C_m^0J_m(n_ckr)e^{im\theta}, \tag{71}$$

and outside cylinder 0,

$$G_{M,ext}(r,\theta)=\sum_{m=-\infty}^{\infty}[A_m^0J_m(n_bkr)+B_m^0Y_m(n_bkr)]e^{im\theta}. \tag{72}$$

The multipole coefficients for the pth cylinder follow from those for the central cylinder using Eq. (2):

$$B_m^p=B_m^0e^{i\mathbf{k}_0\cdot\mathbf{R}_p}. \tag{73}$$

The boundary conditions at the cylinder surface enable the multipole coefficients C_m^0 and A_m^0 to be expressed in terms of B_m^0, and, in particular,

$$A_m^0=-M_mB_m^0, \tag{74}$$

$$M_m=\frac{n_bJ_m(n_ckr_c)Y_m'(n_bkr_c)-n_cJ_m'(n_ckr_c)Y_m(n_bkr_c)}{n_bJ_m(n_ckr_c)J_m'(n_bkr_c)-n_cJ_m'(n_ckr_c)J_m(n_bkr_c)}.$$

The multipole coefficients can be obtained by solving a set of linear equations (the Rayleigh identity)

$$\begin{aligned}M_mB_m^0+\sum_\ell(-1)^{m+\ell}S_{\ell-m}^YB_\ell^0&\\=\frac{1}{4}Y_m(kr_0)e^{-im\theta_0}+\frac{1}{4}\sum_\ell(-1)^{m+\ell}S_{\ell-m}^YJ_\ell(kr_0)e^{-i\ell\theta_0}.&\end{aligned} \tag{75}$$

The two terms on the right-hand side arise, respectively, from the source in the central unit cell and the sources in all other unit cells, reexpressed using Graf's addition theorem. The quantities S_ℓ^Y are sums over the array of cylindrical harmonics phased by the Bloch factor. Once the coefficients B_m^0

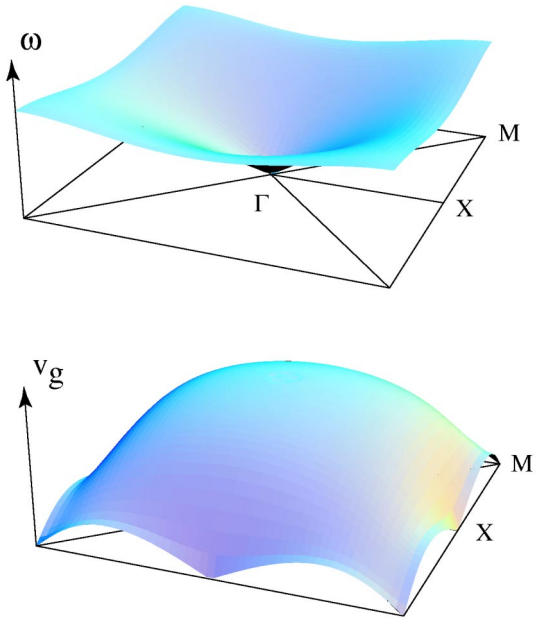

FIG. 3. (Color online) (a) Surface showing the frequency of the acoustic band as a function of the Bloch vector. (b) Surface showing the magnitude of the group velocity divided by c of this mode as a function of the Bloch vector. TM polarization, $a=0.3$, $n_c=3.0$, $n_b=1$, square array of unit period.

are obtained by solving a truncated set of Eqs. (75), the value of $\mathcal{M}$ can be obtained from Eq. (21) using the expansion (72), taking care to subtract the divergent contribution due to the source in the central unit cell.

A similar approach can be used to find photonic crystal modes ψ_m. In this case, the multipole coefficients result from a homogeneous system, there being no source term in the Rayleigh identity:

$$M_m B_m^0 + \sum_\ell (-1)^{m+\ell} S_{\ell-m}^Y B_\ell^0 = 0. \tag{76}$$

For a given value of $\mathbf{k}_0$, the determinant of this identity can be calculated over a given range of values of ω; the zeros of the determinant give the allowed values of $\omega_m(\mathbf{k}_0)$. We can perturb the values of the components k_{0x} and k_{0y} slightly to obtain the corresponding components of the group velocity $\mathbf{v}_g$ by numerical differentiation. By changing the cylinder index n_c slightly, we can obtain $\partial\omega_m/\partial n_c$ by numerical differentiation, and thus evaluate the mode normalization factor $\mathcal{N}$ from Eq. (60). Knowing $\mathbf{v}_g$ and $\mathcal{N}$, we can use Eq. (70) to evaluate the flux density associated with the mode.

In Fig. 3 we show both the variation of ω with Bloch vector across the first Brillouin zone for the acoustic band and the variation of the magnitude of the group velocity $|\mathbf{v}_g|$ across the same region. Note that the acoustic band surface exhibits within the Brillouin zone one maximum, two saddle points, and one minimum, in accord with general arguments given in Callaway [16]. The minimum is at Γ, entirely within the Brillouin zone, and the mode surface there comes to a conical point, with slope given by the effective refractive index of the mode (see below). The two saddle points occur

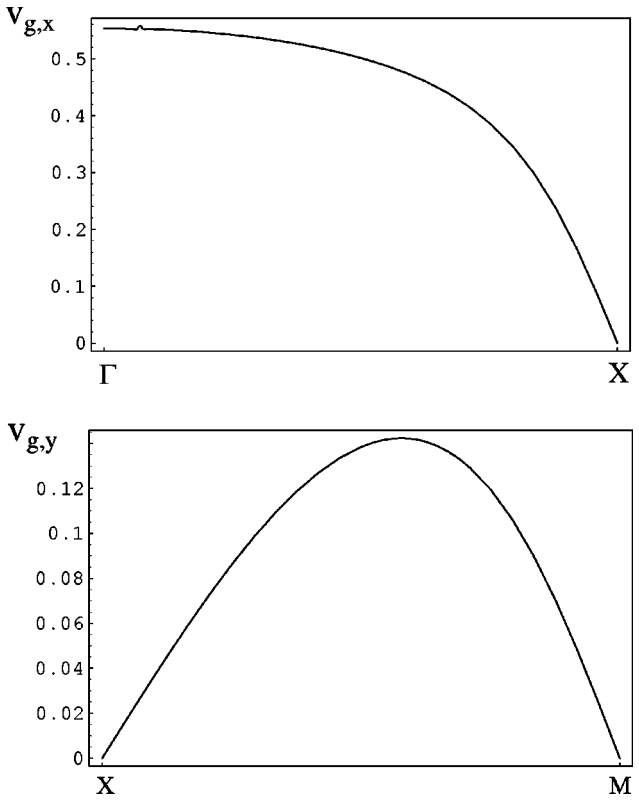

FIG. 4. Detail of Fig. 3 along the lines ΓX (a) and XM (b).

at X and its three equivalent points, with each contributing half of a saddle point to the Brillouin zone. The four corners of the Brillouin zone each contribute one quarter of the maximum to the Brillouin zone. Note that the group velocity vanishes at both X and M.

The sections of the group velocity surface shown in Fig. 4 give the variation of the nonzero Cartesian components of this vector along the symmetry lines ΓX and XM. The value of $\mathbf{v}_g/c$ at Γ is 0.553 68, which agrees to all figures quoted with the reciprocal of the homogenized refractive index for this polarization (see below). The nonzero Cartesian component of $\mathbf{v}_g$ can be seen to change sign at both X and M.

B. SDOS, LDOS, and DOS

To evaluate the SDOS, LDOS, and DOS we can divide the irreducible part of the Brillouin zone into a grid of values $\mathbf{k}_0$. For each of these, we calculate the values for each ω_m, and place them in an array which records those modes lying in specified frequency ranges. Appropriately normalized, this array gives the discretized spectral density function $\mathcal{S}(\omega,\mathbf{k}_0)$. The density of states function $N(\omega)$ results from combining all entries for varying $\mathbf{k}_0$ which lie in the specified frequency ranges. In order to calculate the function $\mathcal{L}(\mathbf{r}_s,\omega)$, we must for each point in a grid covering the Wigner-Seitz cell, according to Eq. (25), accumulate the modulus squared value of the normalized wave function (or wave functions, if more than one corresponds to a given pair of ω and $\mathbf{k}_0$) for all values of $\mathbf{k}_0$ and for each frequency. This is the procedure used by John and Busch [17] to calculate the LDOS at se-

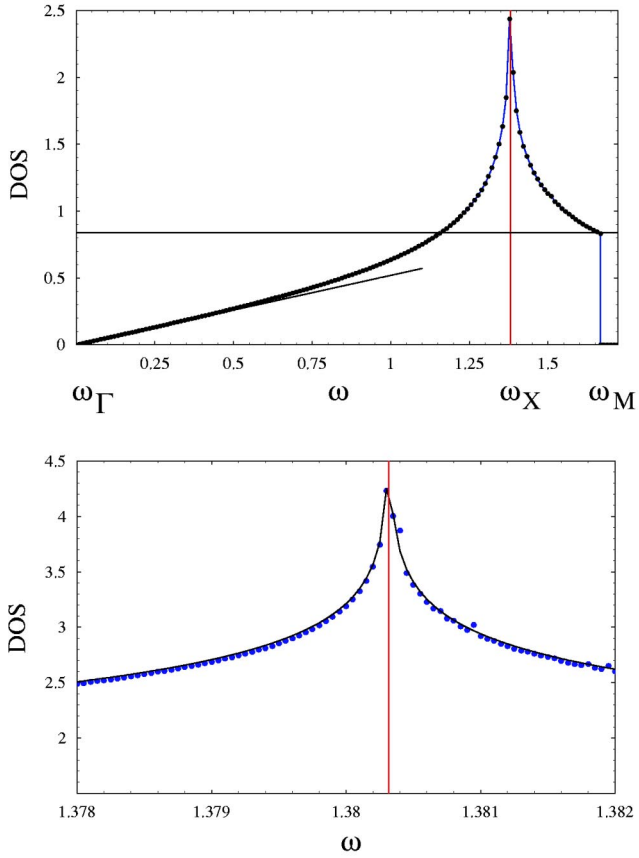

FIG. 5. (Color online) DOS as calculated by numerical integration for the square array, with the points giving the analytic estimates based on Eq. (80), the sloping straight line giving the low frequency asymptote based on the effective index (77), and the horizontal straight line to Eq. (81), for the data of Fig. 3. (a) Whole of the acoustic band, (b) region near X.

lected points in a three-dimensional lattice, and by Moroz [18] for the one-dimensional case.

A second, slightly different method is to take the frequency data corresponding to a grid of values filling the Brillouin zone and to fit a smooth interpolating function to it. This function then enables the construction of isofrequency contours and the group velocity (as shown in Fig. 3) by numerical differentiation. The density of states can then be calculated using Eq. (41), where of course we need only integrate over the segment of the isofrequency contour lying within ΓXM, given the symmetry properties of the integrand evident from Fig. 3.

In Fig. 5 we show the DOS as a function of frequency for the first band of a square array of dielectric cylinders, with the numerical results from either of the above methods agreeing to better than graphical accuracy. There are three regions evident. At low frequencies, the DOS is approximately a linear function of frequency, its slope being determined by the homogenized refractive index n_h, which for this polarization is the result of the linear mixing formula [19]:

$$n_h^2 = \frac{\pi r_c^2 n_c^2 + (d^2 - \pi r_c^2) n_b^2}{d^2}, \tag{77}$$

d being the period of the array. In this region,

$$N_0(\omega) \sim \frac{A_{\mathrm{WSC}} n_h^2 \omega}{2\pi c^2}. \tag{78}$$

Beyond the linear region, the DOS increases sharply, in fact diverging logarithmically [20], before decreasing again and dropping sharply to zero at the edge of the first band gap. There are 1000 points on the curve, and the numerical test of the relationship (44) gives the value 1.000 73 for the first band.

There is an interesting property suggested by Fig. 5. If the low frequency straight line is extrapolated to M, it passes very close to $N_0(\omega_M)$. This is a property which holds for the phonon density of states for the square lattice in two dimensions [8]. However, it does not hold in general for two-dimensional photonic crystals: we have verified numerically that, if the cylinder radius of Fig. 5 is perturbed away from $a=0.3$, the apparent coincidence of the low frequency model with $N_0(\omega_M)$ is removed.

C. DOS and critical points

The behavior of the DOS near its logarithmic peak and at the edge of the band gap can be understood in terms of a critical point analysis, well presented by Bassani and Pastori Parravicini [20]. Around critical points, the photonic bands have a frequency which varies with wave number in quadratic fashion, characterized by effective mass parameters we will denote by C_X and C_Y. The logarithmic peak in fact corresponds to a frequency ω_0 which is the value of ω for the first mode at the end of the segment ΓX—i.e., $\mathbf{k}_0 = (\pi/d, 0)$. The mode surface has a saddle point at X, near which point we approximate its form by

$$\omega = \omega_X - \frac{(\Delta k_X)^2}{2C_X} + \frac{(\Delta k_Y)^2}{2C_Y} + \cdots, \tag{79}$$

where $\Delta k_X = k_{0x} - \pi/d$, $\Delta k_Y = k_{0y}$. We show in Fig. 6 the variation of ω along the symmetry lines ΓX and XM, together with least square fits to the dispersion relation to the left and right of X. These give the numerical estimates at X: $C_X = 1.431$, $C_Y = 8.566$.

We display in Fig. 7 isofrequency contours across a quarter of the Brillouin zone. These are circular near Γ, and become more distorted with increasing frequency. A key feature is evident in Fig. 7, which explains the key difference in the contribution to the DOS of the saddle point X from that of the band maximum M: the length of the isofrequency contours near X tends to a constant, whereas near M it tends to zero. Also given in Fig. 7 are two straight lines starting at X and Y, with respective slopes $-\sqrt{C_Y/C_X}$ and $-\sqrt{C_X/C_Y}$, which indicate the local separators between the contours centerd on Γ and M.

The contribution from this point and the three equivalent points to the DOS is of the form [20]

$$N_0(\omega) = -\frac{4}{A_{\mathrm{BZ}}} \sqrt{C_X C_Y} [\ln|\omega - \omega_X| + C], \tag{80}$$

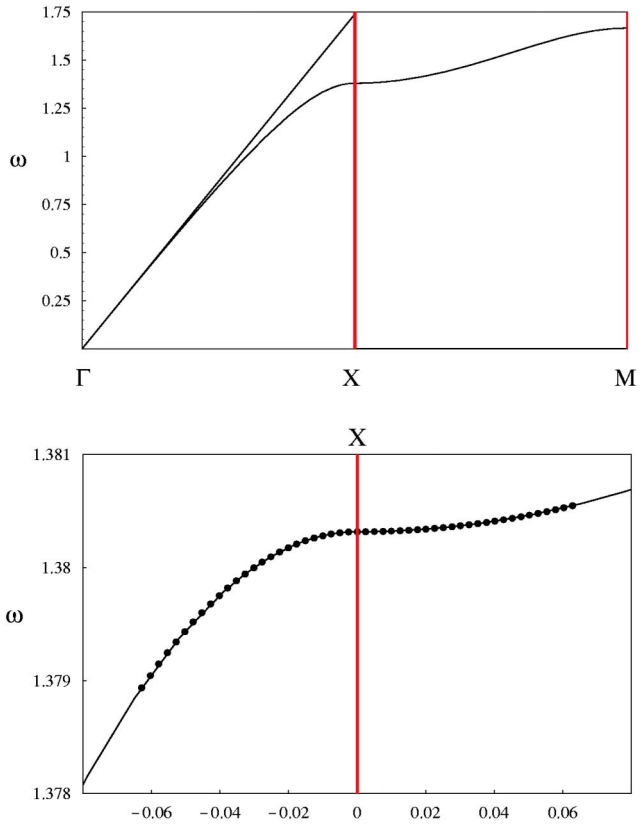

FIG. 6. (Color online) (a) frequency of the acoustic mode along the line ΓXM, with the sloping straight line corresponding to the effective index of Eq. (77). (b) detail near X, showing least squares fits according to Eq. (79), which determine C_X and C_Y at X, for the data of Fig. 3.

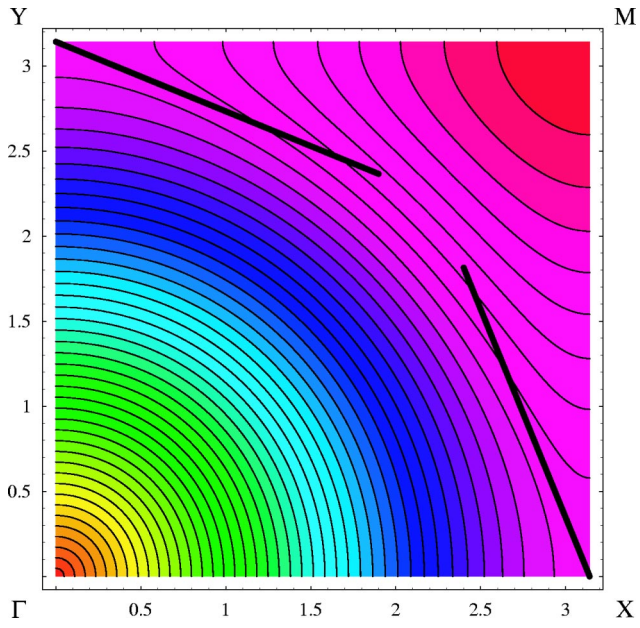

FIG. 7. (Color online) Isofrequency contours for the acoustic band, and straight lines giving local separators of contours near X and Y, for the data of Fig. 3.

for C an additive constant. The comparison of Eq. (80) with the numerical DOS curve shown in Fig. 3 uses the value of best fit $C=-1$.

The local density of states at ω_X is, from Eq. (42), dominated by the contribution from $|\psi_0(X,\mathbf{r}_s)|^2$. As the frequency sweeps through the value corresponding to a critical point, the LDOS becomes proportional to $|\psi|^2$ for that point. Thus, as ω increases from ω_X to ω_M, the spatial pattern of the LDOS evolves from $|\psi_0(X,\mathbf{r}_s)|^2$ to $|\psi_0(M,\mathbf{r}_s)|^2$.

The edge of the band gap occurs at the point M, where $\mathbf{k}_0=(\pi/d,\pi/d)$. This is a maximum of the band surface, and this critical point gives a contribution

$$N_0(\omega)=\frac{C_M d^2}{2\pi}, \tag{81}$$

i.e., we expect the DOS to flatten out at the band edge, before falling steeply to zero in the gap. Note that, for the point M, by symmetry $C_X=C_Y=C_M$, with a least squares fit to the data in Fig. 6 giving $C_M=5.269$. The result (81) is validated in Fig. 5.

Using Eq. (81), the form of the mode surface near M is

$$\omega=\omega_M-\frac{(\Delta k_{xM}^2+\Delta k_{yM}^2)d^2}{4\pi N_0(\omega_M)}+\cdots, \tag{82}$$

where $\Delta k_{xM}=k_{0x}-\pi/d$, $\Delta k_{yM}=k_{0y}-\pi/d$.

D. LDOS

We next consider the local density of states for a specific frequency value. To evaluate this we need to evaluate the integral (42). We have carried out this using a method of calculating flux-normalized Bloch functions [21]. To convert from a Bloch function normalized with respect to (say) the flux $\mathcal{F}_y$ along the y axis to a mode normalized with respect to its electromagnetic energy [as in Eq. (22)], we use Eq. (70), with the result that the integrand in Eq. (42) involves the ratio v_{gy}/v_g rather than $1/v_g$. Note that it is sufficient to carry out the integral along the isofrequency contour over the first quadrant only, by virtue of the symmetry of the square array and the circular inclusion. Figure 8 shows two views of the local density of states, as a function of position in the unit cell. Note that the LDOS strongly peaks in the cylinders, and both its value and its normal derivative are continuous at the cylinder surface, as expected. We can numerically integrate the local density of states weighted by the dielectric constant over the unit cell, to provide a test of Eq. (36). For the frequency of Fig. 8, the numerical integral gave 1.0472, in satisfactory agreement with the independent value (1.0455).

E. Modes at symmetry points

The Rayleigh identity (76) takes an interesting special form at points such as X and M. Since the corresponding $\mathbf{k}_0$ has the property that this and $-\mathbf{k}_0$ are separated by a reciprocal lattice vector, the lattice sums S_ℓ^Y are equal at $\pm\mathbf{k}_0$. Using also the symmetry properties of the square array, we find that the lattice sums are real and $S_{2\ell-1}^Y=0$ for all integers l. The Rayleigh identity then becomes

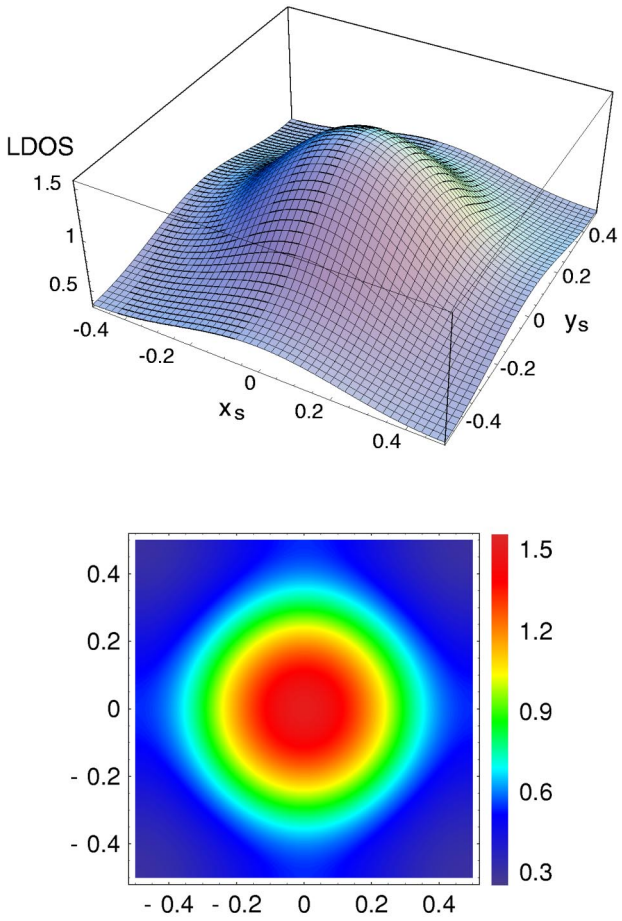

FIG. 8. (Color online) The local density of states for a square array of cylinders ($a=0.3d$, $n_c=3.0$, $\lambda=5.0d$, TM polarization).

$$M_m B_m^0 + \sum_n S_{2n}^Y B_{m+2n}^0 = 0. \tag{83}$$

Equations (83) break into two separate families: the set with even order multipole coefficients and the set with odd order multipole coefficients. As the boundary condition terms M_m are real, the multipole coefficients in either case may be taken to be real, and they have the property that $B_{-m} = (-1)^m B_m$. The potential expansions for the even solution inside and outside the central cylinder are

$$\psi_{int}(r,\theta) = \sum_{m=-\infty}^{\infty} \varepsilon_{2m} C_{2m}^0 J_{2m}(n_c kr)\cos(2m\theta), \tag{84}$$

$$\psi_{ext}(r,\theta) = \sum_{m=-\infty}^{\infty} \varepsilon_{2m}[A_{2m}^0 J_{2m}(n_b kr) + B_{2m}^0 Y_{2m}(n_b kr)]\cos(2m\theta), \tag{85}$$

where $\varepsilon_{2m}=1$ if $m=0$ and 2 otherwise. All the coefficients A, B, and C here are real, as is the function ψ. The odd solution is similar, except that $2m$ is replaced by $2m-1$. However, this difference enables us to see that the odd solution must be zero at the center of the high index region, while the even solution is nonzero there (given the coefficient B_0 is nonzero). We thus expect, as is in fact evident from numerical results [22], the even solution to correspond to a lower frequency than the odd solution, with the former giving a point on the acoustic band surface and the latter a point on the optical band surface.

The Bloch factor $\exp(i\mathbf{k}_0\cdot\mathbf{R}_p)$ for point X is $\exp(i\pi p_x)$, where $\mathbf{R}_p = d(p_x, p_y)$. Using this to connect the values of ψ in adjacent unit cells, we can deduce the following properties of the even solution:

$$\frac{\partial\psi_e(X;x,y)}{\partial y} = 0 \quad \text{on } y = 0, \pm d, \ldots,$$

$$y = \pm d/2, \pm 3d/2, \ldots,$$

$$\frac{\partial\psi_e(X;x,y)}{\partial x} = 0 \quad \text{on } x = 0, \pm d, \ldots,$$

$$\psi_e(X;x,y) = 0 \quad \text{on } x = \pm d/2, \pm 3d/2, \ldots,$$

$$\psi_e(X;x,y) = \psi_e(X;x,-y) = \psi_e(X;-x,y) = \psi_e(X;-x,-y)$$
$$\text{for } (x,y) \in (\text{WSC}). \tag{86}$$

The Bloch factor $\exp(i\mathbf{k}_0\cdot\mathbf{R}_p)$ for point M is $\exp i\pi(p_x + p_y)$, where $\mathbf{R}_p = d(p_x, p_y)$, so that for this value of $\mathbf{k}_0$ we obtain similar properties to Eq. (86) along lines at 45° to the x and y axes.

The odd solution has the following properties at X:

$$\frac{\partial\psi_o(X;x,y)}{\partial y} = 0 \quad \text{on } y = 0, \pm d, \ldots,$$

$$y = \pm d/2, \pm 3d/2, \ldots,$$

$$\frac{\partial\psi_0(X;x,y)}{\partial x} = 0 \quad \text{on } x = \pm d/2, \pm 3d/2, \ldots,$$

$$\psi_o(X;x,y) = 0 \quad \text{on } x = 0, \pm d, \ldots,$$

$$\psi_o(X;x,y) = \psi_o(X;x,-y) = -\psi_o(X;-x,y) = -\psi_o(X;-x,-y) \quad \text{for } (x,y) \in (\text{WSC}). \tag{87}$$

The symmetry conditions (86) and (87) ensure that for both the even and odd modes the energy flux density $\psi^* \partial\psi/\partial n$ vanishes at each point on the boundary of the Wigner-Seitz cell.

There is an interesting special case for TM polarization in which an analytic solution may be found for the lowest band near Γ, which does not give a band surface with the conical form of Fig. 2. This case is that of the square array of perfectly conducting cylinders, which has been studied by a number of authors [23–26]. The dispersion equation for the acoustic band is

$$\omega=\omega_\Gamma+\frac{(\Delta k_0)^2c^2}{2\omega_\Gamma}+\cdots, \tag{88}$$

where, because we are expanding about Γ, $\Delta k_0=k_0$ and

$$\omega_\Gamma^2=\frac{2\pi c^2}{d^2}\left[\ln\frac{r_c}{d}+\mathcal{C}\right]^{-1}+\cdots, \tag{89}$$

with $\mathcal{C}=1.310\,532\,92$ [25] for the square array. This band then has a minimum at Γ, which marks the top edge of a band gap starting at $\omega=0$. The form of Eq. (82) for this band minimum is

$$\omega=\omega_\Gamma+\frac{(\Delta k_0)^2d^2}{4\pi N_0(\omega_\Gamma)}+\cdots, \tag{90}$$

and so

$$N_0(\omega_\Gamma)=\frac{\omega_\Gamma d^2}{2\pi c^2}+\cdots. \tag{91}$$

Thus, in this particular case, we have an analytic estimate giving the density of states at the top edge of the first gap in terms of the frequency there, with that frequency also being determined analytically by Eq. (89). As $r_c\to 0$, both ω_Γ and $N_0(\omega_\Gamma)$ tend to zero slowly, as the square root of the inverse of the logarithm.

VI. TE POLARIZATION

We give here the necessary changes to the key formulas of Secs. II and III for the case of TE polarization. We denote the Bloch modes for this polarization by $\Psi_m(\mathbf{k}_0,\mathbf{r})$, and we require at the cylinder boundaries that Ψ and $(1/\varepsilon)\partial\Psi/\partial n$ be continuous. The appropriate form of the Helmholtz equation, true in the sense of distributions, is then [27]

$$\boldsymbol{\nabla}\cdot\left(\frac{1}{n^2(\mathbf{r})}\boldsymbol{\nabla}\Psi_m(\mathbf{k}_0,\mathbf{r})\right)+\frac{\omega_m^2}{c^2}\Psi_m(\mathbf{k}_0,\mathbf{r})=0. \tag{92}$$

This then results in the inner product form replacing Eq. (9),

$$\langle\Psi_l,\Psi_m\rangle_H=\int_{\mathrm{WSC}}\Psi_l(\mathbf{k}_0,\mathbf{r})\Psi_m^*(\mathbf{k}_0,\mathbf{r})d^2\mathbf{r}. \tag{93}$$

Hence, the appropriate expansion for G_M is now

$$G_M(\mathbf{r},\mathbf{r}_s;\omega,\mathbf{k}_0)=\sum_l\frac{\Psi_l^*(\mathbf{k}_0,\mathbf{r}_s)\Psi_l(\mathbf{k}_0,\mathbf{r})}{[\omega^2-\omega_l^2(\mathbf{k}_0)]/c^2}. \tag{94}$$

The other key equations follow, generally, by omitting the weighting factor of the dielectric constant which occurred for TM polarization:

$$\mathcal{L}_H(\mathbf{r}_s;\omega)=-\frac{2\omega}{\pi c^2}\mathrm{Im}[\mathbf{G}(\mathbf{r}_s,\mathbf{r}_s;\omega)]\ \mathcal{U}_H, \tag{95}$$

where G and G_M are related by Eq. (20) and where the normalization factor is now very simple:

$$\mathcal{U}_H=\int_{\mathrm{WSC}}d^2\mathbf{r}_s=A_{\mathrm{WSC}}. \tag{96}$$

The mutual density of states for this polarization is

$$\begin{aligned}\mathcal{M}_H(\mathbf{r}_s,\omega,\mathbf{k}_0)&=-\frac{2\omega}{\pi c^2}\mathrm{Im}[G_M(\mathbf{r}_s,\mathbf{r}_s,\omega,\mathbf{k}_0)]\ \mathcal{U}_H\\&=\sum_m\delta(\omega-\omega_m(\mathbf{k}_0))|\Psi_m(\mathbf{k}_0,\mathbf{r}_s)|^2\ \mathcal{U}_H.\end{aligned} \tag{97}$$

The local density of states is now

$$\mathcal{L}_H(\mathbf{r}_s,\omega)=\frac{\mathcal{U}_H}{A_{\mathrm{BZ}}}\sum_m\int_{\mathrm{BZ}}d^2\mathbf{k}_0\,\delta(\omega-\omega_m(\mathbf{k}_0))|\Psi_m(\mathbf{k}_0,\mathbf{r}_s)|^2, \tag{98}$$

where this function and $1/\varepsilon(\mathbf{r})$ times its normal derivative are continuous across interfaces. It obeys the governing equation

$$\begin{aligned}&\boldsymbol{\nabla}\cdot\left[\frac{1}{n^2(\mathbf{r})}\boldsymbol{\nabla}\mathcal{L}_H(\mathbf{r}_s,\omega)\right]+2\frac{\omega^2}{c^2}\mathcal{L}_H(\mathbf{r}_s,\omega)\\&\quad=\frac{2\mathcal{U}_H}{n^2(\mathbf{r})A_{\mathrm{BZ}}}\sum_m\int_{\mathrm{BZ}}\delta(\omega-\omega_m)\\&\qquad\times\boldsymbol{\nabla}\Psi_m(\mathbf{k}_0,\mathbf{r}_s)\cdot\boldsymbol{\nabla}\Psi_m^*(\mathbf{k}_0,\mathbf{r}_s)d^2\mathbf{k}_0,\end{aligned} \tag{99}$$

where $\omega_m=\omega_m(\mathbf{k}_0)$. The spectral density of states is

$$\begin{aligned}\frac{1}{\mathcal{U}_H}\int_{\mathrm{WSC}}\mathcal{M}_H(\mathbf{r}_s,\omega,\mathbf{k}_0)d^2\mathbf{r}_s&=\sum_m\delta(\omega-\omega_m(\mathbf{k}_0))\\&=\mathcal{S}_H(\mathbf{k}_0,\omega),\end{aligned} \tag{100}$$

and is connected to the Dyson Green function again:

$$\begin{aligned}\mathcal{S}_H(\mathbf{k}_0,\omega)&=\frac{-2\omega\mathcal{U}_H}{\pi c^2}\mathrm{Im}[G_D(\omega,\mathbf{k}_0)]\\&=\frac{-2\omega}{\pi}\mathrm{Im}\sum_m\frac{1}{[\omega^2-\omega_m^2(\mathbf{k}_0)]}.\end{aligned} \tag{101}$$

The total density of states is

$$N(\omega)=\frac{1}{\mathcal{U}_H}\int_{\mathrm{WSC}}\mathcal{L}_H(\mathbf{r}_s,\omega)d^2\mathbf{r}_s=\frac{1}{A_{\mathrm{BZ}}}\int_{\mathrm{BZ}}\mathcal{S}(\mathbf{k}_0,\omega)d^2\mathbf{k}_0. \tag{102}$$

Its integral form over isofrequency lines is once again given by Eq. (41), while the corresponding integral for the LDOS is

$$\mathcal{L}_H(\mathbf{r}_s,\omega)=\mathcal{U}_H\sum_m \frac{1}{A_{\mathrm{BZ}}}\int_{C(\omega_m)}\frac{|\Psi_m(\mathbf{k}_0,\mathbf{r}_s)|^2}{v_g}dk_{0t}. \tag{103}$$

With these results, the necessary changes to other equations in Secs. III, IV, and V are obvious, with perhaps two exceptions. The first is the derivation of the result equivalent to Eq. (55),

$$\mathcal{N}_H=\int_{U_+}|\Psi_m|^2dA+\int_{U_-}|\Psi_m|^2dA$$
$$=\frac{-\omega_m}{n_c\partial\omega_m/\partial n_c}\left[\int_{U_-}|\Psi_m|^2dA+\frac{c^2}{\omega_m^2 n_c^2}\int_{C_-}\Psi_m\frac{\partial\Psi_m^*}{\partial n}dl\right]. \tag{104}$$

Using Green's first formula, this can be written as

$$\left(\frac{\partial\omega_m}{\partial n_c}\right)\mathcal{N}_H=-\frac{\omega_m}{n_c}\int_{U_-}\nabla\Psi_m\cdot\nabla\Psi_m^*dA. \tag{105}$$

Once again, we can conclude that the effect of increasing the cylinder refractive index is to lower the frequency of all photonic bands (irrespective of the shape of the cylinders).

A second subtlety concerns the formula for the effective dielectric constant of the array at long wavelengths. This is no longer given by Eq. (77), but [19,28] is given by the Maxwell-Garnett formula in the dipole approximation:

$$n_h^2=n_b^2\left[1+\frac{2f}{(n_c^2+n_b^2)/(n_c^2-n_b^2)-f}\right], \tag{106}$$

where $f=\pi r_c^2/d^2$. Higher order formulas for this effective dielectric constant may be found by multipole methods. Note that the derivation of Eq. (106) involves the application of Keller's theorem for two-dimensional composite materials [19,29,30], since the boundary conditions for TE polarization involve reciprocal dielectric constants, whereas those customary in electrostatics for the calculation of effective dielectric constant involve the dielectric constants without inversion.

VII. CONCLUSION

We have seen that the mutual density of states provides a formal framework for the construction of the other density of states functions (LDOS, SDOS, and DOS). The MDOS may be calculated conveniently as the response of a periodic array of cylinders to a phased array of sources, which requires only the evaluation of the field in one unit cell rather than for multiple unit cells. Thus, it may also be viewed as providing a computational factorization for the calculation of density of states functions, well adapted to an efficient implementation on parallel computers.

The analytic connections we have exhibited between the form of mode surfaces for two-dimensional systems and the variation with frequency of the density of states seem powerful and interesting for applications of photonic crystals.

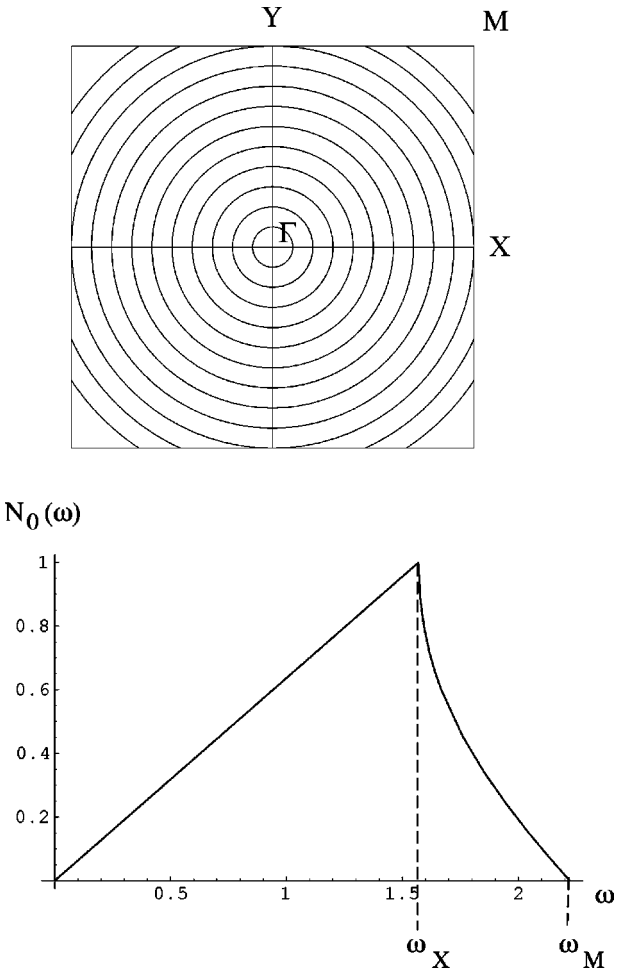

FIG. 9. (a) isofrequency contours for the lowest band of the square array, in the case of the empty lattice. (b) the corresponding density of states ($n_h=2$).

The DOS for the acoustic band has been shown to be characterized by four numbers: an effective index for low frequencies (which can be calculated from known expressions in the homogenization literature), two band curvatures for the point *X*, and one for the point *M*. Analytic knowledge concerning these band curvatures would thus be of great value.

The steep variation of the DOS between frequencies corresponding to *X* and *M* may well offer interesting design trade-offs. Near *X*, the density of states is very high, but a single frequency corresponds to a wide range of wave vectors. Near *M*, each frequency corresponds to a tight range of wave vectors, and one has the advantage of operating just on the low frequency side of an absolute band gap, but the density of states is not high.

Additional insights may well flow from the study of densities of states for higher bands and for geometries of photonic crystals other than the single case studied here.

ACKNOWLEDGMENTS

The support of the Australian Research Council for the Centre of Excellence for Ultrahigh-bandwidth Devices for

Optical Systems is acknowledged. Helpful inputs from Dr. Kurt Busch and Dr. Geoff Smith are acknowledged.

APPENDIX: THE EMPTY LATTICE

The simplest exemplification of the various density of states functions is provided in the case of the empty lattice, where we put $n_c = n_b = n_h$. Using Eqs. (1) and (4), we see that

$$G_M(\mathbf{r},\mathbf{r}_s;\omega,\mathbf{k}_0) = \frac{1}{A_{\mathrm{WSC}}} \sum_h \frac{e^{i\mathbf{Q}_h\cdot(\mathbf{r}-\mathbf{r}_s)}}{\left(\frac{\omega^2 n_h^2}{c^2} - Q_h^2\right)}. \quad \text{(A1)}$$

From Eqs. (14) and (21), we see that

$$\mathcal{M}(\mathbf{r}_s,\omega,\mathbf{k}_0) = \sum_h \delta\left(\omega - \frac{cQ_h}{n_h}\right), \quad \text{(A2)}$$

which is in keeping with the normalized wave function

$$\psi_h(\mathbf{r}) = \frac{e^{i\mathbf{Q}_h\cdot\mathbf{r}}}{n_h\sqrt{A_{\mathrm{WSC}}}}. \quad \text{(A3)}$$

We can use Eq. (A2) to get the SDOS,

$$\mathcal{S}(\mathbf{k}_0,\omega) = \sum_h \delta\left(\omega - \frac{cQ_h}{n_h}\right). \quad \text{(A4)}$$

The LDOS is

$$\mathcal{L}(\mathbf{r}_s,\omega) = \frac{1}{A_{\mathrm{BZ}}}\int_{\mathrm{BZ}} d^2\mathbf{k}_0 \sum_h \delta\left(\omega - \frac{cQ_h}{n_h}\right) = \frac{n_h}{A_{\mathrm{BZ}}c}\int_{\mathrm{BZ}} d^2\mathbf{k}_0 \sum_h \delta\left(Q_h - \frac{n_h\omega}{c}\right). \quad \text{(A5)}$$

We split this up into its contributions from each band h, and define the length of the isofrequency contour in the Brillouin zone for band h at frequency ω to be $L_h(\omega)$. Then, from the second integral in Eq. (A5):

$$\mathcal{L}_h(\mathbf{r}_s,\omega) = \frac{L_h(\omega)n_h}{A_{\mathrm{BZ}}c}. \quad \text{(A6)}$$

Hence, from Eq. (36), the density of states for band h is

$$N_h(\omega) = \frac{1}{\mathcal{U}}\int_{\mathrm{WSC}} \varepsilon(\mathbf{r}_s)\mathcal{L}(\mathbf{r}_s,\omega)d^2\mathbf{r}_s = \frac{n_h}{A_{\mathrm{BZ}}c}L_h(\omega). \quad \text{(A7)}$$

As asserted, the DOS and the LDOS agree for a uniform dielectric. Further, to check Eq. (44),

$$\int_{\text{band } h} N_h(\omega)d\omega = \frac{n_h}{A_{\mathrm{BZ}}c}\int_{\text{band } h} L_h(\omega)d\omega = 1, \quad \text{(A8)}$$

since the second integral has the value $A_{\mathrm{BZ}}c/n_h$.

As a specific example, for the lowest or acoustic band, and for the square array of period d:

$$L_0(\omega) = \frac{2\pi n_h\omega}{c}, \quad \text{for } \omega \leqslant \frac{\pi c}{dn_h} = 4\left[\frac{\pi}{2} - 2\cos^{-1}\left(\frac{\pi c}{n_h\omega d}\right)\right]\left(\frac{n_h\omega}{c}\right) \quad \text{(A9)}$$

for $\pi c/(dn_h) \leqslant \omega \leqslant \sqrt{2}\pi c/(dn_h)$. Hence,

$$N_0(\omega) = \frac{A_{\mathrm{WSC}}n_h^2\omega}{2\pi c^2}, \quad \text{for } \omega \leqslant \frac{\pi c}{dn_h} = \frac{A_{\mathrm{WSC}}n_h^2\omega}{2\pi c^2}\left[1 - \frac{4}{\pi}\cos^{-1}\left(\frac{\pi c}{n_h\omega d}\right)\right] \quad \text{(A10)}$$

for $\pi c/(dn_h) \leqslant \omega \leqslant \sqrt{2}\pi c/(dn_h)$. Isofrequency contours and the DOS for this case are shown in Fig. 9.

[1] J. P. Dowling, H. Everitt, and E. Yablonovitch, http://home.earthlink.net/~jpdowling/pbgbib.html.
[2] S. John, Phys. Rev. Lett. **58**, 2486 (1987).
[3] E. Yablonovitch, Phys. Rev. Lett. **58**, 2059 (1987).
[4] O. Painter, R.K. Lee, A. Scherer, A. Yariv, J.D. O'Brien, P.D. Dapkus, and I. Kim, Science **284**, 1819 (1999).
[5] G.S. Agrawal, Phys. Rev. A **11**, 230 (1975).
[6] S. Doniach and E. H. Sondheimer, *Green's Functions for Solid State Physicists* (Benjamin, London, 1974).
[7] E. N. Economou, *Green's Functions in Quantum Physics* (Springer-Verlag, Berlin, 1983).
[8] Ping Sheng, *Introduction to Wave Scattering, Localization, and Mesoscopic Phenomena* (Academic Press, San Diego, 1995).
[9] M.L. Glasser and J. Boersma, J. Phys. A **33**, 5017 (2000).
[10] H.P. Zidek and A.R. Baghai-Wadji, Electron. Lett. **30**, 915 (1994).
[11] A. Lagendijk and B.A. van Tiggelen, Phys. Rep. **270**, 143 (1996).
[12] D. S. Jones, *Generalized Functions* (McGraw-Hill, New York, 1966).
[13] G. Allaire, C. Conca, and M. Vanninathan, ESAIM: Proceedings of the 29th Congress of Numerical Analysis:CANum'97 (unpublished) URL:http://www.emath.fr/proc/vol.3.
[14] C. Kittel, *Introduction to Solid State Physics* (Wiley, New York, 1976).
[15] C. Poulton, R. C. McPhedran, L. C. Botten, and N. A. Nicorovici, in *IUTAM Symposium on Asymptotics, Singularities and Homogenisation in Problems of Mechanics*, edited by A.B. Movchan (Kluwer, Dordrecht, 2003).
[16] J. Callaway, *Quantum Theory of the Solid State* (Academic, New York, 1974).
[17] S. John and K. Busch, J. Lightwave Technol. **17**, 1931 (1999).

[18] A. Moroz, Europhys. Lett. **46**, 419 (1999).
[19] G. W. Milton, *The Theory of Composites* (Cambridge University Press, Cambridge, 2001).
[20] F. Bassani and G. Pastori Parravicini, *Electronic States and Optical Transitions in Solids* (Pergamon Press, London, 1975).
[21] L.C. Botten, N.A. Nicorovici, R.C. McPhedran, C.M. de Sterke, and A.A. Asatryan, Phys. Rev. E **64**, 046603 (2001).
[22] J. D. Joannopoulos, R. D. Meade, and J. N. Winn, *Photonic Crystals* (Princeton University Press, Princeton, 1995).
[23] J.B. Pendry, A.J. Holden, W.J. Stewart, and I. Youngs, Phys. Rev. Lett. **76**, 4773 (1996).
[24] M.J. Ward and J.B. Keller, SIAM (Soc. Ind. Appl. Math.) J. Appl. Math. **53**, 770 (1993).
[25] N.A. Nicorovici, R.C. McPhedran, and L.C. Botten, Phys. Rev. E **52**, 1135 (1995).
[26] D. Felbacq and G. Bouchitté, Waves Random Media **7**, 245 (1997).
[27] *Electromagnetic Theory of Gratings* edited by R. Petit, (Springer-Verlag, Berlin, 1980).
[28] W.T. Perrins, D.R. McKenzie, and R.C. McPhedran, Proc. R. Soc. London, Ser. A **369**, 207 (1979).
[29] N.A. Nicorovici, R.C. McPhedran, and L.C. Botten, Phys. Rev. Lett. **75**, 1507 (1995).
[30] A.A. Krokhin, P. Halevi, and J. Arriaga, Phys. Rev. B **65**, 115208 (2002).